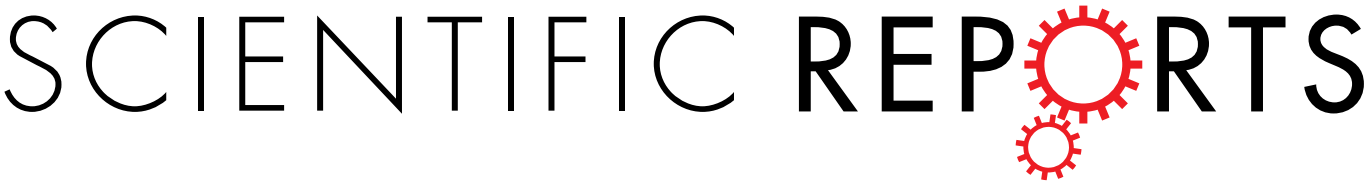

OPEN

High-field transport properties of a P-doped $BaFe_2As_2$ film on technical substrate

Received: 22 July 2016
Accepted: 30 November 2016
Published: 12 January 2017

Kazumasa Iida[1], Hikaru Sato[2], Chiara Tarantini[3], Jens Hänisch[4], Jan Jaroszynski[3], Hidenori Hiramatsu[2,5], Bernhard Holzapfel[4] & Hideo Hosono[2,5]

High temperature (high-T_c) superconductors like cuprates have superior critical current properties in magnetic fields over other superconductors. However, superconducting wires for high-field-magnet applications are still dominated by low-T_c Nb_3Sn due probably to cost and processing issues. The recent discovery of a second class of high-T_c materials, Fe-based superconductors, may provide another option for high-field-magnet wires. In particular, *AE*Fe_2As_2 (*AE*: Alkali earth elements, *AE*-122) is one of the best candidates for high-field-magnet applications because of its high upper critical field, H_{c2}, moderate H_{c2} anisotropy, and intermediate T_c. Here we report on in-field transport properties of P-doped $BaFe_2As_2$ (Ba-122) thin films grown on technical substrates by pulsed laser deposition. The P-doped Ba-122 coated conductor exceeds a transport J_c of 10^5 A/cm^2 at 15 T for main crystallographic directions of the applied field, which is favourable for practical applications. Our P-doped Ba-122 coated conductors show a superior in-field J_c over MgB_2 and NbTi, and a comparable level to Nb_3Sn above 20 T. By analysing the $E-J$ curves for determining J_c, a non-Ohmic linear differential signature is observed at low field due to flux flow along the grain boundaries. However, grain boundaries work as flux pinning centres as demonstrated by the pinning force analysis.

The discovery of Fe-based superconductors (FBS) by Kamihara *et al.*[1], brought a huge impact to the physics community, since the compound consists of ferromagnetic Fe, which had been believed to be inevitably detrimental to the formation of Cooper pairs. To date, fundamental questions, such as mechanism of Cooper pairing and order parameter symmetry, are still under debate[2]. On the other hand, this material class is attractive for applications. For instance, *AE*Fe_2As_2 (*AE*: Alkali earth elements, *AE*-122) and Fe(Se, Te) possess high upper critical fields (H_{c2}) exceeding 50 T and a low H_{c2} anisotropy close to 1 at low temperature[3,4], which is favourable for high-field-magnet applications. Furthermore, Ba-122 shows less deterioration of critical current across grain boundaries (GBs)[5,6] than $YBa_2Cu_3O_{7-\delta}$ (YBCO) and Bi-based cuprates. For Co-doped Ba-122, the critical GB misorientation angle (θ_c), where J_c starts to fall off exponentially, has been reported to be $6° - 9°$ [5,7]. Even high angle GBs do not impede the current flow very much in sintered K-doped Ba-122 wires and bulks, if clean and well-connected GBs are realised[8,9]. Additionally, Co-doped Ba-122 exhibits a high tolerance for large densities of flux pinning centres in the superconducting matrix, which leads to significant increase in critical current density (J_c) and irreversibility field (H_{irr})[10].

Another advantage of Ba-122, in particular P-doped Ba-122, is its inherently high J_c. Putzke *et al.* have reported on the enhancement of the vortex core energy of the flux lines at the quantum critical point (QCP) of the antiferromagnetic phase[11]. Indeed, even microstructurally clean and optimally P-doped Ba-122 epitaxial thin films, which were prepared by molecular beam epitaxy (MBE), exhibit a high self-field J_c of over 6 MA/cm^2 at 4.2 K[12]. Although excess magnetic Fe has been found to be harmful to superconductivity in Fe(Se, Te)[13], Fe-rich P-doped Ba-122 thin films showed a higher self-field J_c of over 10 MA/cm^2 at 4.2 K, which is the highest value ever

[1]Department of Crystalline Materials Science, Nagoya University, Chikusa-ku, Nagoya 464-8603, Japan. [2]Laboratory for Materials and Structures, Institute of Innovative Research, Tokyo Institute of Technology, Mailbox R3-1, 4259 Nagatsuta-cho, Midori-ku, Yokohama 226-8503, Japan. [3]Applied Superconductivity Center, National High Magnetic Field Laboratory, Florida State University, Tallahassee FL 32310, USA. [4]Karlsruhe Institute of Technology, Institute for Technical Physics, Hermann-von-Helmholtz-Platz 1, 76344 Eggenstein-Leopoldshafen, Germany. [5]Materials Research Center for Element Strategy, Tokyo Institute of Technology, Mailbox SE-6, 4259 Nagatsuta-cho, Midori-ku, Yokohama 226-8503, Japan. Correspondence and requests for materials should be addressed to K.I. (email: iida@nuap.nagoya-u.ac.jp)

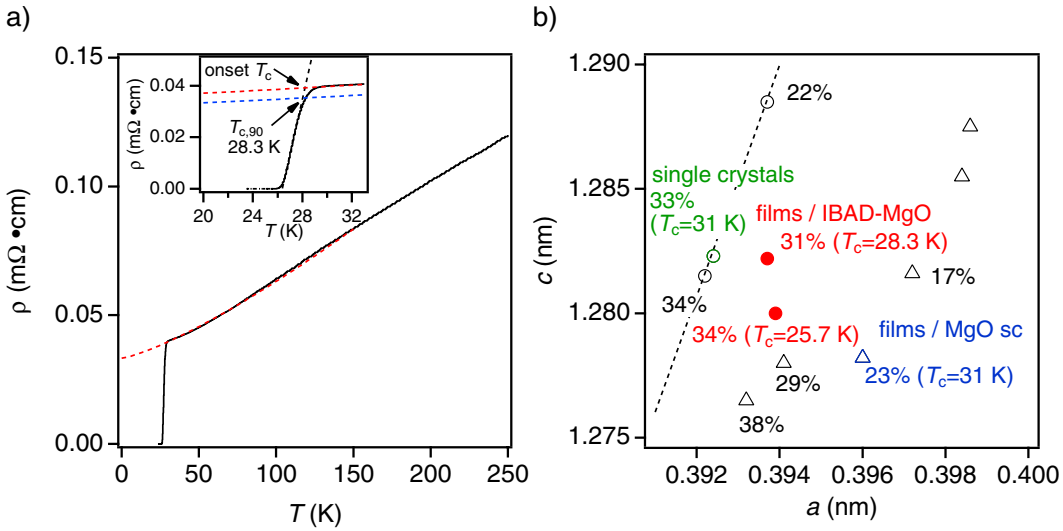

Figure 1. Resistivity and the relationship between structural parameters and T_c. (**a**) Temperature dependence of the resistivity measured in the absence of magnetic field. The dotted red line is a fit of the normal state resistivity curve in the range of $30 < T < 150$ K using $\rho_n = \rho_0 + AT^n$. Inset: resistivity near the superconducting transition. The dotted blue line is a 90% reduction of the fitting curve (red dotted line). A $T_{c,90}$ of 28.3 K was recorded. (**b**) The relationship between lattice parameters a and c for P-doped Ba-122 single crystals[22] and thin films on MgO single crystal substrates[24] for various P contents. The highest-T_c values for single crystal and thin film are obtained by a P content of 33% and 23%, respectively. Lattice parameters a and c of our P-doped Ba-122 thin films on IBAD-MgO (two samples) are located between single crystals and thin films deposited on MgO single crystalline substrates. Both films have almost comparable $\Delta\phi_{Ba122}$ and $\Delta\omega_{Ba122}$ values.

reported for FBS[6]. Whereas in the former case Fe is incorporated interstitially[14], in the latter case the Fe may form Fe-containing particles or regions with differing P-content, both acting as pinning centres[6]. Furthermore, the high J_c and low anisotropy P-doped Ba-122 thin films can be fabricated by tuning the processing conditions only, without any modification of the target material used in pulsed laser deposition (PLD)[15].

The aforementioned advantages of P-doped Ba-122 are very suitable for high-field-magnet applications. Indeed, P-doped Ba-122 thin films on technical substrates have been demonstrated as FBS coated conductors[16,17]. To date, two kinds of technical substrates have been employed for FBS coated conductors: The cube-textured metal tapes with buffer layers (i.e., RABiTS)[18] and the Hastelloy tape on which biaxially textured buffer layers are prepared by ion-beam-assisted-deposition (IBAD)[19].

In contrast to Fe(Se, Te) coated conductors[20,21], transport properties of P-doped Ba-122 coated conductors in the presence of extremely high magnetic fields have not yet been reported. Here, we report on in-field transport properties of a P-doped Ba-122 thin film grown by PLD on metal substrate with biaxially textured MgO template (IBAD-MgO) in a wide range of temperature and DC magnetic field up to 35 T. We employ IBAD-MgO template with a relatively large in-plane full width at half maximum (FWHM) value ($\Delta\phi_{MgO} = 8°$), since it has been demonstrated by x-ray diffraction (XRD) and transmission electron microscope (TEM) characterisations that the texture of MgO is transferred to the overlying P-doped Ba-122 film, generating dislocation networks[17]. Such dislocation networks enhance the vortex pinning in P-doped Ba-122[17], since θ_c is less than 9°[5]. Indeed, in-field J_c properties of our P-doped Ba-122 on IBAD-MgO with $\Delta\phi_{MgO} = 8°$ were superior to those of the film on a template with $\Delta\phi_{MgO} = 4°$[17]. A high density of threading dislocations is very effective for improving J_c for $H||c$ in a wide range of temperature and magnetic field even close to H_{irr}. Despite the relatively large θ_c of 6°–9° for Ba-122, J_c of our P-doped Ba-122 coated conductor with sharp FWHM values of both in-plane, $\Delta\phi_{Ba-122} = 5.7°$, and out-of-plane misorientaion, $\Delta\omega_{Ba-122} = 1.2°$ (see Supplemental Fig. S1) is limited by the GBs in the low field regime. However, at high field, it exceeds a transport J_c of 10^5 A/cm^2 at 15 T for field applied in both main crystallographic directions. Our P-doped Ba-122 coated conductor sample shows superior in-field J_c properties over MgB_2 and NbTi, and a comparable level to Nb_3Sn above 20 T.

Results

Resistivity measurements. The normal-state resistivity ρ_n (Fig. 1a) can be approximated by $\rho_n = \rho_0 + AT^n$ with an exponent n-value of 1.28, $\rho_0 = 3.32 \times 10^{-2}$ mΩ·cm and $A = 8.22 \times 10^{-5}$ mΩ·cm/K$^{1.28}$ in the range of $30 < T < 150$ K in accord with ref. 22. Shibauchi *et al.* have reported that the exponent n is unity at the quantum critical point (QCP) of the antiferromagnetic phase, where the maximum T_c is observed at 33% of P content for bulk single crystals[23]. Based on those results, we infer that the P content of our Ba-122 thin film on IBAD-MgO is different from the optimal level. Chemical analysis by electron probe microanalysis revealed a P content of 0.31, high enough to induce superconductivity with an onset T_c of 30 K for Ba-122 single crystal[22]. The lower T_c (28.3 K) of the P-doped Ba-122 coated conductor may be a consequence of epitaxial strain, since MgO single crystalline

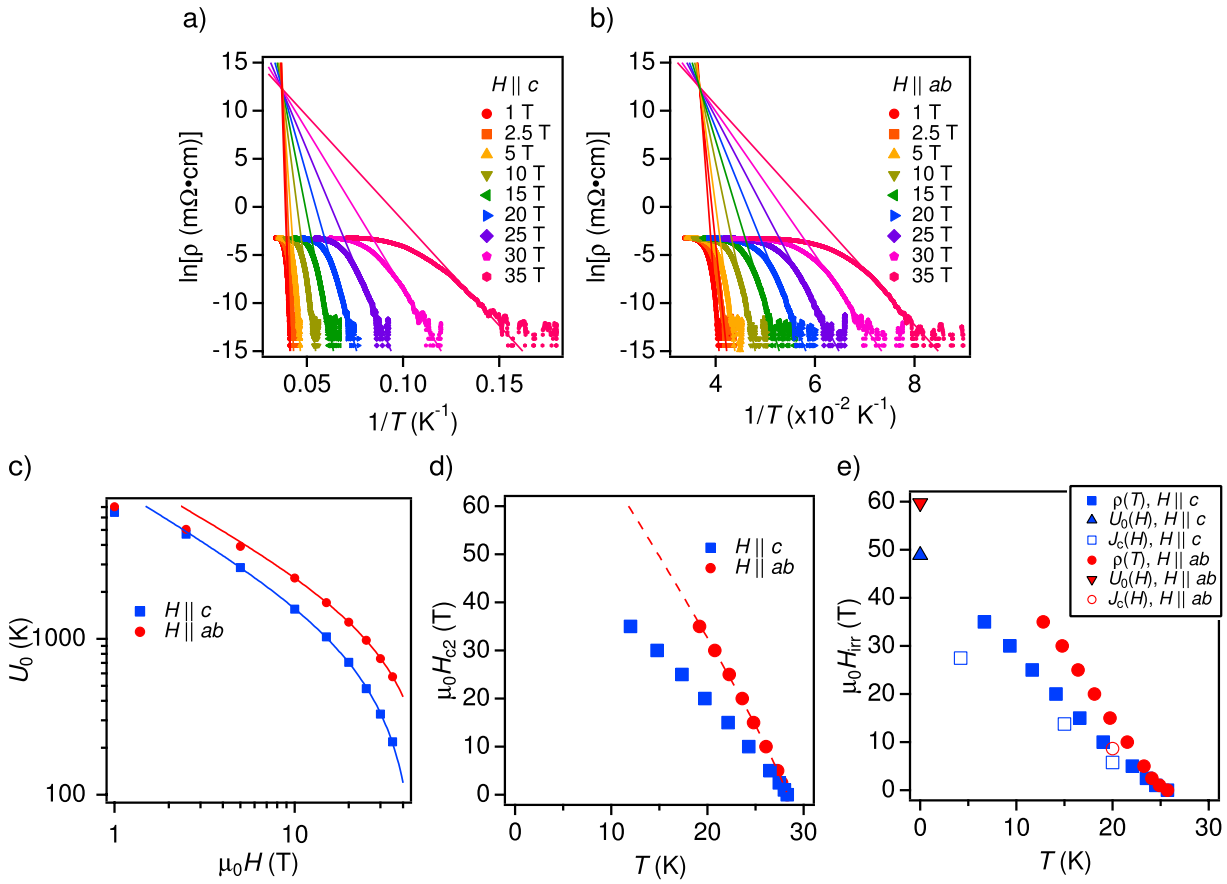

Figure 2. Analysis of the activation energy for pinning potential, the upper critical field and the irreversibility field. Arrhenius plots of the resistivity curves for (**a**) $H||c$ and (**b**) $H||ab$. (**c**) Field dependence of the pinning potential for both main crystallographic directions. (**d**) Temperature dependence of the upper critical field for both major directions. (**e**) Temperature dependence of the irreversibility field for both major directions evaluated from $\rho(T, H)$ and $J_c(T, H)$ measurements. Zero temperature H_{irr} for $H||c$ and $||ab$ evaluated from $U_0(H)$ is also shown.

substrates induce in-plane tensile strain to Ba-122 films due to a large lattice mismatch[24,25]. The lattice parameters a and c of our P-doped Ba-122 coated conductors are located between the single crystals and thin films deposited on MgO single crystalline substrates (Fig. 1b). The crystalline quality of IBAD-MgO affects mainly $\Delta\phi_{Ba122}$ rather than $\Delta\omega_{Ba122}$[17], changing the amount of the in-plane strain and hence T_c.

The linearity of the Arrhenius plots of $\rho(T, H)$ for both major crystallographic directions at a certain magnetic field (Fig. 2a and b) reveals thermally activated flux motion under the assumption of a linear T-dependence of the activation energy, $U_0(H)$[26] (See the method section). It can be seen from Fig. 2c that $U_0(H)$ for both $H||c$ and $||ab$ are well described by $H^{\alpha}(1 - H/H^*)^{\beta}$ above 10 T, which has been used for analysing polycrystalline MgB_2 samples by Thompson *et al.*[27] H^* is a characteristic field representing the irreversibility field at 0 K[27,28]. The evaluated values for $H||c$ and $||ab$ are 48.9 T and 59.7 T, respectively (for $H||c$ and $||ab$ $\alpha = 0.68$ and 0.64, and $\beta = 1.1$ and 0.94).

A linear fit for $\ln\rho(H)$ versus $U_0(H)$ using $\ln\rho_0(H) = \ln\rho_{0f} + U_0(H)/T_c$, where ρ_{0f} is the prefactor, yields T_c of 26.9 K for $H||c$ and 27.2 K for $H||ab$, respectively (see Supplemental Fig. S2a). The T_c values evaluated by this method are slightly lower than the $T_{c,90}$ (see Fig. 1a). A plausible explanation for this difference is the increased transition width ΔT_c due to the reduced texture quality compared to films on single crystal substrates or single crystal samples.

$H_{c2}(T)$ was evaluated from the linear presentations of Fig. 2a and b (see Supplementary Fig. S2b and S2c) applying a $\rho_{n,0.9} = 0.9\rho_n$ resistivity criterion, where $\rho_{n,0.9}$ is the normal state resistivity ρ_n at 28.5 K. Shown in Fig. 2d is H_{c2} for $H||c$ and $||ab$. The dotted line in Fig. 2d is the fitting curve using $(1 - T/T_c)^k$. An exponent k of 0.9 was obtained for $H||ab$, which is far from the expected value of 0.5 for layered compounds limited by Pauli pair breaking at given T close to the dimensional crossover temperature[29–31], which confirms that P-doped Ba-122 is a 3D superconductor. Because of the lack of low temperature data, it is not possible to fit the $H_{c2}(T)$ (and $H_{c2}(\theta)$, shown later unambiguously) with a proper model for FBS[32,33].

The temperature dependence of the irreversibility field, $H_{irr}(T)$ (Fig. 2e) was evaluated from $\rho(T, H)$ measurements using a resistivity criterion of $\rho_c = E_c/J_{c,100} = 1.0^{-8}\,\Omega\cdot$cm, where E_c is the electric field criterion (1 μV/cm) for determining J_c from $E - J$ measurements and $J_{c,100}$ is the criterion (100 A/cm^2) for determining H_{irr} from $J_c(H)$ measurements (see Supplementary Fig. S2d and S2e). The H_{irr} data at 0 K are estimated from the Arrhenius plots and they appear to match the low temperature limit of the H_{irr} data directly determined from the $\rho(T, H)$ using

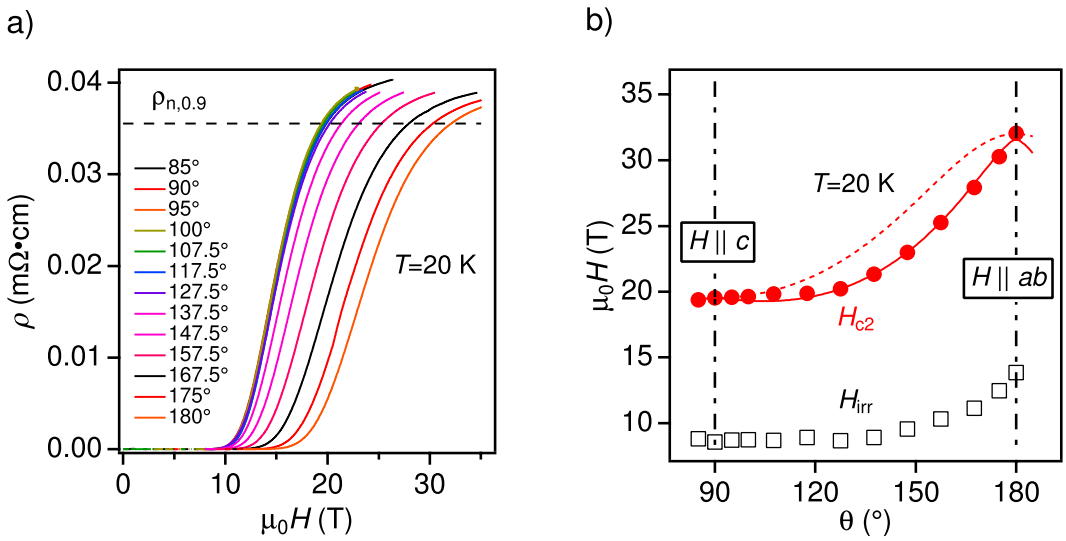

Figure 3. Angular dependence of the upper critical field and the irreversibility field. (**a**) Angular dependence of magnetoresistivity [$\rho(H)$] at 20 K up to 35 T. (**b**) Angular dependence of the upper critical field and the irreversibility field at 20 K. The solid line is the fitting curve using eq. (1) with $\delta = 1.47$ and $\gamma = 1.62$. The dotted line is the AGL dependence.

the ρ_c criterion. For comparison, $H_{irr}(T)$ determined from $J_c(H)$ is also plotted in Fig. 2e showing some differences with the values estimated from $\rho(T, H)$. A plausible reason is a different frequency of the applied current used in those investigations[34].

The angular dependence of H_{c2} at 20 K, which was derived from $\rho(H)$ curves at constant angles with $\rho_{n,0.9}$ (Fig. 3a) shows a minimum at $\theta = 90°$ ($H||c$) and a maximum at $\theta = 180°$ ($H||ab$), as shown in Fig. 3b. The single-band anisotropic Ginzburg-Landau (AGL) theory[35], $H_{c2}(\theta) = H_{c2}(90°)(\sin^2(\theta) + \cos^2(\theta)/\gamma^2)^{-0.5}$ with $\gamma = H_{c2}(180°)/H_{c2}(90°)$ (dotted line in Fig. 3b), cannot describe the measured $H_{c2}(\theta)$ due to the multi-band nature of this material, similarly to Co-doped Ba-122[28]. A fairly good description of the data is, however, achieved by the empirical formulae[28],

$$H_{c2}(\theta) = H_{c2}(90^\circ) \times \epsilon(\theta, \gamma, \delta),\ \epsilon(\theta, \gamma, \delta) = \left(|\sin\theta|^{\delta} + \left|\frac{\cos\theta}{\gamma}\right|^{\delta} \right)^{-\frac{1}{\delta}} \quad (1)$$

with $\delta = 1.47$ and $\gamma = 1.62$ (solid line). The parameter γ is the H_{c2} anisotropy, whereas δ is a measure for the *ab*-peak width whose physical meaning is still unclear. These two values will be used later for scaling the angular dependence of $J_c(\theta)$ data.

The angular dependence of H_{irr} at 20 K derived using the same resistivity criterion $\rho_c = 1.0^{-8}\,\Omega\cdot$cm shows almost the same trend as $H_{c2}(\theta)$. Unlike the angular dependence of J_c (see next section), no clear peak at $\theta = 90°$ ($H||c$) is observed in $H_{irr}(\theta)$.

In-field critical current density $J_c(T, H, \theta)$. The $E - J$ curves of the P-doped Ba-122 coated conductor sample at 4.2 K (Fig. 4) show different behaviour at high and low magnetic fields for both major field directions. Up to 10 T they exhibit a non-Ohmic linear differential (NOLD) signature (i.e., E is linearly changing with J in linear scale, see Supplemental Fig. S3), indicative of J_c limitation by GBs[36]. Here NOLD behaviour is due to viscous flux flow along the GBs[37]. On the other hand, NOLD signature is almost absent above 12.5 T, suggesting that J_c is limited by intra-grain depinning of flux lines. This pinning crossover field is observed to decrease with increasing temperature (not shown), which is consistent with the cuprate YBCO reported in refs 38,39.

Figure 5a compares $J_c(H)$ for P-doped Ba-122 on IBAD-MgO for $H||c$ at 4.2 K with P-doped Ba-122 on MgO single crystalline substrate[15], Fe(Se, Te) on RABiTS[21], YBCO coated conductor[40], MgB_2[41], NbTi[42,43], and Nb_3Sn[44,45]. Pinning-improved YBCO 2nd-generation (2G) tape shows the highest J_c at entire magnetic fields, however, a well textured template is necessary. The P-doped Ba-122 coated conductor exceeds a self-field J_c of 4 MA/cm^2 and maintains a high J_c value of 50 kA/cm^2 at 20 T. For the entire field range, J_c of P-doped Ba-122 coated conductor sample is larger than for MgB_2 and NbTi. Above 20 T, the P-doped Ba-122 coated conductor sample shows comparable properties to Nb_3Sn. Although lower-field J_c of P-doped Ba-122 on IBAD-MgO is higher than that of Fe(Se, Te) on RABiTS, the latter shows the better performance at medium and high fields. Figure 5b summarises $J_c(H)$ for P-doped Ba-122 on IBAD-MgO for both crystallographic directions at various temperatures. At intermediate fields J_c for the two directions is comparable, indicative of the presence of correlated pinning along the *c*-axis.

By analysing the pinning force density $F_p = \mu_0 H \times J_c$, information on vortex pinning can be obtained. In general, the normalised pinning force, $f_p = F_p/F_{p,max}$, is plotted as a function of reduced field $h_1 = H/H_{irr}$ at a given

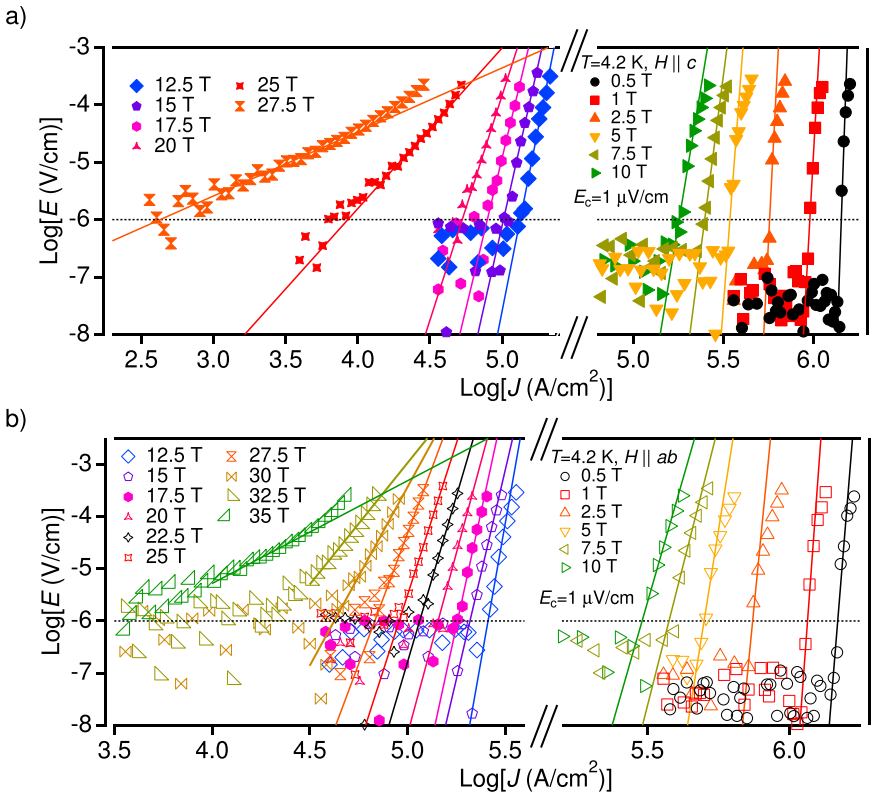

Figure 4. ***E*** **−** ***J*** **characteristics.** $E-J$ curves for P-doped Ba-122 measured at 4.2 K for (**a**) $H||c$ in the range of $0.5 < \mu_0 H < 27.5$ T and (**b**) for $H||ab$ in the range of $0.5 < \mu_0 H < 35$ T. The electric field criterion of 1 μV/cm for evaluating J_c is also shown. A NOLD signature can be identified at low field by the deviation from the linear trend observed at high E.

temperature for high-T_c superconductors. However, we plot f_p as a function of $h = H/H_{max}$, where H_{max} is the field at which F_p shows the maximum[46–49], since J_c could not be measured up to H_{irr} at all temperatures. As can be seen in Fig. 5c, the f_p curves at different temperatures for $H||c$ almost fall onto a master curve in the range of $0 < h < 3$ described by

$$f_p = \frac{25}{16} h^{0.5} \left(1 - \frac{h}{5}\right)^2 \quad (2)$$

This formula is analogous to $h_1^p(1 - h_1)^q$ ($p = 0.5$ and $q = 2$) found by Dew-Hughes[50] for pinning by planar defects such as GB and twin boundaries, and by Kramer for line defect arrays[51]. In high-T_c superconductors with extremely short coherence lengths ξ, a further classification of the defect size with respect to ξ is necessary. It has been recently found by Paturi *et al.* that the exponent p is 0.5 irrespective of q for a defect size of the order of ξ and especially for dislocations in undoped YBCO films[49]. On the contrary, p increases towards 1 with increasing defect size. This confirms the finding that pinning in our sample is dominated by the dislocations with nano-size. Here, it should be noted that a sign of NOLD signature does not contradict GB pinning. In fact it has been reported for YBCO that the dislocations in GBs can work as vortex pinning centres[52,53]. The flux preferentially flows across the dislocation cores in the GB plane, which explains the $E-J$ curves with a NOLD sign.

Abrikosov-Josephson vortices (AJV) are present in low-angle GBs in both YBCO[54] and FBS. Unlike Josephson vortices (JV), AJV have normal cores and can be trapped by flux pinning. Furthermore, the presence of an interaction between Abrikosov vortices (AV) in the grain and AJV at the GBs has been experimentally found in ref. 55: an increase in pinning potential for AV leads to the enhancement of the pinning potential for AJV.

For $H||ab$ the f_p curves at both 10 and 15 K follow well the GB pinning line (red solid line) up to 16 T (corresponding to $h = 2$ and 3.2 in Fig. 5d, respectively). In contrast, f_p at 20 K neither follows the GB pinning nor point-like pinning (red solid and blue dashed lines, respectively) in high field regime, although the f_p curve lies on the GB pinning line below $h < 2$. Similarly, the f_p curve at 4.2 K follows the GB pinning curve up to $h < 1.5$ and then approaches the point-like pinning curve beyond $h > 1.5$. Hence, differently from the $H||c$ case, the dominant pinning mechanism for $H||ab$ is varying with temperature and field strength.

The angular dependence of the critical current density, $J_c(\theta)$ (Fig. 6a–d), shows two distinct peaks: a relatively sharp peak at $H||ab$ and a broad maximum at $H||c$, which arises from the network of threading dislocations comprising the low-angle GBs[17]. Surprisingly, the c-axis peaks [$J_c(90°)$] remain visible even close to H_{irr} at all temperatures. Unlike single band superconductors, the anisotropy of coherence length, $\gamma_\xi = \xi_{ab}/\xi_c$, and penetration depth, $\gamma_\lambda = \lambda_c/\lambda_{ab}$, of FBS exhibit opposite behaviour with temperature[56]. For an optimally doped Ba-122 system,

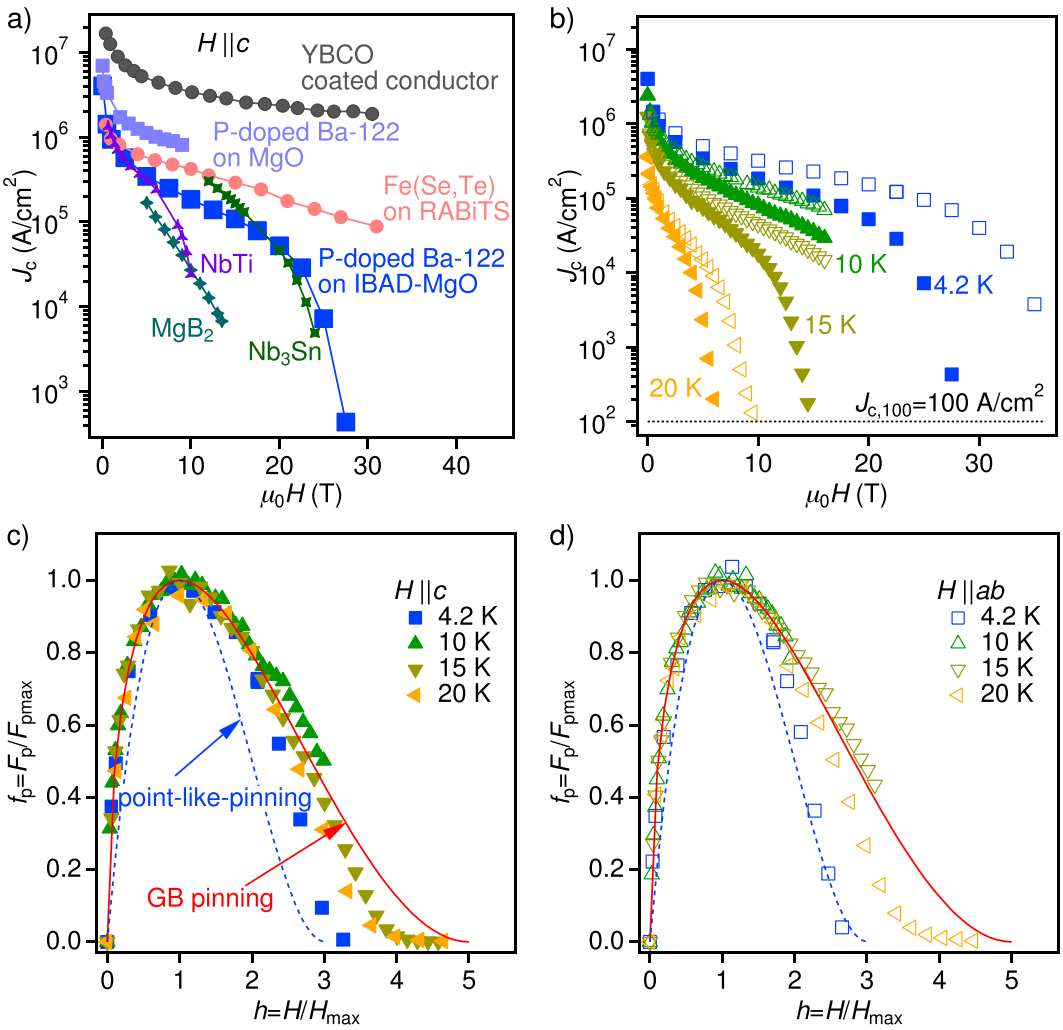

Figure 5. Field dependence of J_c and analysis of the flux pinning density. (**a**) $J_c - H$ properties of the P-doped Ba-122 coated conductor sample at 4.2 K for $H||c$ in comparison to the data for P-doped Ba-122 on MgO single crystalline substrate[15], Fe(Se, Te) on RABiTS[21], YBCO coated conductor[40], MgB_2[41], NbTi[42,43], and Nb_3Sn[44,45]. (**b**) $J_c - H$ properties of the P-doped Ba-122 coated conductor sample at various temperatures for both $H||c$ (closed symbols) and $H||ab$ (open symbols). $J_{c,100}$ is the criterion (100 A/cm^2) used for determining H_{irr}. (**c** and **d**) The normalised pinning force f_p as a function of reduced field h. The solid line is $f_p = \frac{25}{16}h^{0.5}(1 - \frac{h}{5})^2$ for GB pinning, and the blue dotted line represent point-like pinning, $f_p = \frac{9}{4}h(1 - \frac{h}{3})^2$.

$\gamma_\lambda > \gamma_\xi$ holds at all temperature. In this case even occasional uncorrelated defects slightly larger than ξ yield a strong c-axis pinning[57]. Such an effect in combination with threading dislocations along the c-axis may enhance enormously the average pinning potential for applied fields parallel to the c-axis.

Shown in Fig. 6e is the scaling behaviour of $J_c(\theta)$ as a function of the effective field [i.e., $\epsilon(\theta, \gamma, \delta) \times \mu_0 H$] at 20 K. Here $\delta = 1.47$ and $\gamma = 1.62$ were used as obtained by the $H_{c2}(\theta)$ fit. As can be seen, all $J_c(\theta)$ curves collapse onto a master curve in a wide angular range around $H||ab$. Differences between the master curve and the measured $J_c(H)$ for $H||c$ are correlated pinning contributions. Here we emphasise that the J_c peak at $\theta = 180°$ is fully determined by the electronic anisotropy at 20 K and no intrinsic pinning or pinning by planar defects is observed.

Discussions and Conclusions

In order to realise FBS coated conductors, high J_c values with low anisotropy in high fields are necessary. J_c of our P-doped Ba-122 coated conductor nearly reached the practical level of ~0.1 MA/cm^2 at 15 T for any applied field directions at 4.2 K [see Fig. 5a)], which shows superior properties over MgB_2 and NbTi. Above 20 T the level of J_c is comparable to Nb_3Sn. Additionally, the intrinsic anisotropy estimated at 20 K from the H_{c2} data is below 2. Moreover the correlated defects increase J_c for $H||c$ substantially suppressing the effective J_c anisotropy.

As stated above, the inequality of ξ and λ anisotropy in combination with a large density of threading dislocations along the c-axis significantly enhances the average pinning potential. It is worth mentioning that the

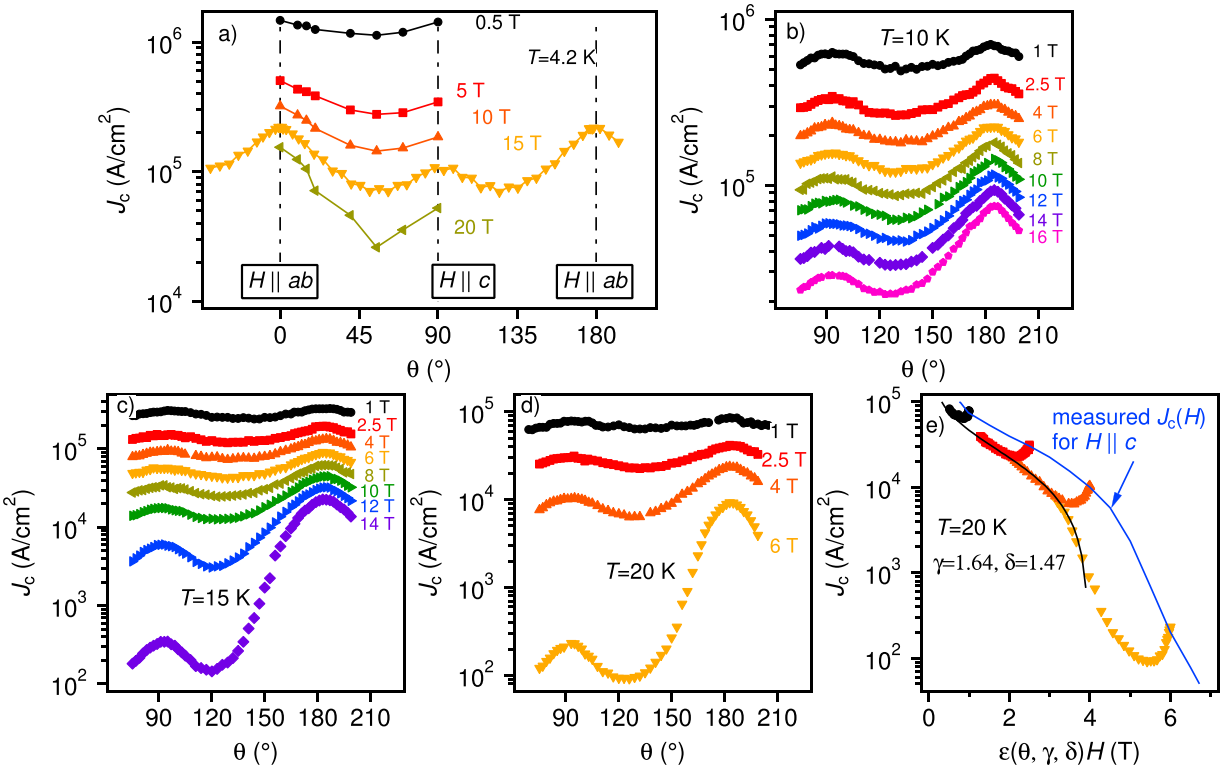

Figure 6. Field and orientation dependence of J_c. Angular dependence of J_c measured at (**a**) 4.2 K, (**b**) 10 K, (**c**) 15 K, and (**d**) 20 K. (**e**) Scaling behaviour of $J_c(\theta)$ at 20 K as a function of effective field, $\epsilon(\theta, \gamma, \delta) \times \mu_0 H$. $\delta = 1.47$ and $\gamma = 1.62$ evaluated from the $H_{c2}(\theta)$ were used. Blue solid line is the measured $J_c - H$ for $H||c$ at 20 K.

population of threading dislocations can be controlled by the processing conditions only, without any modification of the PLD target[15].

Compared to optimally P-doped Ba-122 films on MgO single crystal substrates by MBE[12] and PLD[15], the level of J_c of the P-doped Ba-122 coated conductor still needs to be improved. Film stoichiometry especially for P content should be controlled precisely. As stated before, the P content of our Ba-122 film slightly differs from the optimal level, where the QCP causes a sharp maximum for the vortex core energy[11]. As a consequence, the slight deviation from the optimal P level in our sample results in a lower vortex core energy, which directly reduces J_c.

Unlike in electron and hole doped Ba-122 systems, aliovalent disorder that contributes to pinning in the Co or K cases is absent in P-doped Ba-122. However, J_c can be further enhanced by introducing growth defects (e.g. intragrain dislocations since the PLD processing conditions strongly affect their density[15]) and artificial structures (e.g. nanoparticles). Moreover the thermal conductivity of single crystalline MgO is different from that of IBAD-MgO template, which infers the optimum deposition temperature may change.

The introduction of artificial pinning centres is effective for further improvement of J_c. In fact, Miura *et al.* have reported the introduction of $BaZrO_3$ into P-doped Ba-122 matrix[58] in analogy to the addition of $BaZrO_3$ to YBCO. Hence, a combination of the introduction of artificial pinning centres and the precise control of P content will yield better performing P-doped Ba-122 coated conductors.

An attempt to fabricate a long length P-doped Ba-122 coated conductor has started quite recently. As a result, a 15 cm long P-doped Ba-122 coated conductor has been realised by PLD using a reel-to-reel system[16]. Albeit the resultant P-doped Ba-122 showed a small self-field I_c of 0.47 mA (corresponding to a J_c of 4.7×10^4 A/cm^2) at 4.2 K, an improvement of I_c is foreseen by applying the aforementioned methods.

In summary, we have investigated in-field transport properties of a P-doped Ba-122 thin film grown by PLD on technical substrate in a wide range of temperature and DC magnetic field up to 35 T. The P-doped Ba-122 coated conductor exceeds a transport J_c of 10^5 A/cm^2 at 15 T for both major crystallographic directions of the applied field. Additionally, the J_c peaks for $H||c$ remain visible even close to H_{irr} at all temperatures by the enhanced vortex pinning due to the combination of large population of threading dislocations and the inequality of ξ and λ anisotropy. This leads to a lower J_c anisotropy. By analysing pinning force densities, we established that the GB pinning contribution is dominant for $H||c$, whereas for $H||ab$, the dominant pinning is varying with temperature. The results obtained through this study are considered promising for future high-field-magnet applications of *AE*-122 systems.

Methods

Growth of the P-doped Ba-122 film and structural characterisation. The P-doped Ba-122 thin film of 185 nm thickness was grown by pulsed laser deposition on an IBAD-MgO Hastelloy metal-tape substrate supplied by iBeam Materials, Inc[59]. The stacking structure of the IBAD-MgO substrate, as shown in ref. 17

consists of first a planarising bottom bed-layer amorphous Y_2O_3 on the Hastelloy, second a biaxially textured MgO layer formed by IBAD, and a top homoepitaxial MgO layer. The IBAD-MgO substrate with a large in-plane distribution angle of $\Delta\phi_{MgO} = 8°$ was investigated because higher J_c with isotropic properties can be achieved compared to the film on the well in-plane-aligned IBAD-MgO metal-tapes (i.e., $\Delta\phi_{MgO} = 4°$)[17]. A polycrystalline $BaFe_2(As_{0.65}P_{0.35})_2$ disk was used as the PLD target. We employed a higher growth temperature of 1200 °C than for optimised P-doped Ba-122 films on MgO single-crystal substrates (1050 °C)[15], since the P concentration increases with increasing growth temperature for a given target composition. As expected, a higher P concentration closer to the optimum P concentration than in previous studies was achieved[15,17]. The other growth parameters [e.g., the excitation source and the laser fluence of the second harmonics (wavelength: 532 nm) of a Nd-doped yttrium-aluminum-garnet pulsed laser and 3 J/cm^2, respectively] were the same as reported in ref. 15.

To determine the crystalline phases, ω-coupled 2θ scan X-ray diffraction measurements were performed. The asymmetric 103 diffraction of the P-doped Ba-122 film was measured to confirm the in-plane crystallographic four-fold symmetry without in-plane rotational domains. The crystallinity of the film was characterised on the basis of the full widths at half maximum (FWHMs) of the out-of-plane 004 ($\Delta\omega$) and the in-plane 200 rocking curves ($\Delta\phi$). The results of those XRD measurements can be found in Supplementary Information Fig. S1. The chemical composition was determined with an electron-probe microanalyser. The acceleration voltage of the electron beam was optimised while monitoring the Ni Kα spectrum to avoid the matrix effect from the Ni-containing Hastelloy metal-tapes.

In-plane transport measurements. A small bridge of 15 μm width and 500 μm length was patterned by photolithography, followed by ion-beam etching. Au electrodes with 50 nm thickness were formed by sputtering and lift-off. Transport properties using the resultant bridge were measured by a standard four-probe method.

The temperature dependence of the resistivity of the P-doped Ba-122 coated conductor shows a $T_{c,90}$ of 28.3 K (Fig. 1a), which is about 3 K lower than that of the optimally P-doped Ba-122 single crystals. $T_{c,90}$ is defined as the intersection between the steepest slope of the superconducting transition and a 90% reduction of the fit of the normal state resistivity using $\rho_n = \rho_0 + AT^n$. On the other hand, the onset T_c is defined as the intersection between the fit curve as stated above and the steepest slope of the superconducting transition. The difference between $T_{c,90}$ and the onset T_c is negligible.

The activation energy $U_0(H)$ for vortex motion was evaluated by the temperature dependence of the resistivity measurements in various field strengths up to DC 35 T at the National High Magnetic Field Laboratory, Tallahassee, FL, USA. According to the model of thermally activated flux flow[26], the slope of linear fit yields the pinning potential for vortex motion at given fields (Fig. 2c). On the assumption that $U(T, H) = U_0(H)(1 - T/T_c)$, both equations, $\ln\rho(T, H) = \ln\rho_0(H) - U_0(H)/T$ and $\ln\rho_0(H) = \ln\rho_{0f} + U_0(H)/T_c$, are obtained, where ρ_{0f} is a prefactor.

In order to further understand the H_{c2} anisotropy for a P-doped Ba-122 coated conductor sample, the angular dependence of the magnetoresistivity was measured at 20 K. Using the same constant criterion $\rho_{n,0.9}$ for evaluating H_{c2}, the angular dependent upper critical field [$H_{c2}(\theta)$] was derived (Fig. 3b).

A criterion of 1 μV/cm was employed for evaluating J_c. In J_c measurement, the magnetic field was always applied in the maximum Lorentz force configuration. Low-field measurements were performed in a Quantum Design physical property measurement system (PPMS) in magnetic fields up to 16 T. For high field measurements up to DC 35 T, the experiments were conducted at the National High Magnetic Field Laboratory, Tallahassee, FL, USA.

References

1. Kamihara, Y. *et al.* Iron-Based Layered Superconductor La[$O_{1-x}F_x$]FeAs ($x = 0.05$–0.12) with $T_c = 26$ K. *J. Am. Chem. Soc.* **130,** 3296–3297 (2008).
2. Hirschfeld, P. J. Using gap symmetry and structure to reveal the pairing mechanism in Fe-based superconductors. *C.R. Physique* **17,** 197–231 (2016).
3. Yamamoto, A. *et al.* Small anisotropy, weak thermal fluctuations, and high field superconductivity in Co-doped iron pnictide $Ba(Fe_{1-x}Co_x)_2As_2$. *Appl. Phys. Lett.* **94,** 062511 (2009).
4. Lei, H. *et al.* Pauli-limited upper critical field of $Fe_{1+y}Te_{1-x}Se_x$. *Phys. Rev. B* **81,** 094518 (2010).
5. Katase, T. *et al.* Advantageous grain boundaries in iron pnictide superconductors. *Nat. Commun.* **2,** 409 (2011).
6. Sakagami, T. *et al.* Critical current density and grain boundary property of $BaFe_2(As,P)_2$ thin films. *Physica C* **494,** 181–184 (2013).
7. Lee, S. *et al.* Weak-link behavior of grain boundaries in superconducting $Ba(Fe_{1-x}Co_x)_2As_2$ bicrystals. *Appl. Phys. Lett.* **95,** 212505 (2009).
8. Weiss, J. D. *et al.* High intergrain critical current density in fine-grain $(Ba_{0.6}K_{0.4})Fe_2As_2$ wires and bulks. *Nat. Mater.* **11,** 682–685 (2012).
9. Weiss, J. D. *et al.* Demonstration of an iron-pnictide bulk superconducting magnet capable of trapping over 1 T. *Supercond. Sci. Technol.* **28,** 112001 (2015).
10. Tarantini, C. *et al.* Development of very high J_c in $Ba(Fe_{1-x}Co_x)_2As_2$ thin films grown on CaF_2. *Sci. Rep.* **4,** 7305 (2014).
11. Putzke, C. *et al.* Anomalous critical fields in quantum critical superconductors. *Nat. Commun.* **5,** 5679 (2014).
12. Kurth, F. *et al.* Unusually high critical current of clean P-doped $BaFe_2As_2$ single crystalline thin film. *Appl. Phys. Lett.* **106,** 072602 (2015).
13. Bendele, M. *et al.* Tuning the superconducting and magnetic properties of $Fe_ySe_{0.25}Te_{0.75}$ by varying the iron content. *Phys. Rev. B* **82,** 212504 (2010).
14. Sun, Y. *et al.* Dynamics and mechanism of oxygen annealing in $Fe_{1+y}Te_{0.6}Se_{0.4}$ single crystal. *Sci. Rep.* **4,** 4585 (2014).
15. Sato, H., Hiramatsu, H., Kamiya, T. & Hosono, H. High critical-current density with less anisotropy in $BaFe_2(As,P)_2$ epitaxial films: Effect of intentionally grown *c*-axis vortex-pinning centers. *Appl. Phys. Lett.* **104,** 182603 (2014).
16. Hosono, H. *et al.* Exploration of new superconductors and functional materials, and fabrication of superconducting tapes and wires of iron pnictides. *Sci. Technol. Adv. Mater.* **16,** 033503 (2015).
17. Sato, H., Hiramatsu, H., Kamiya, T. & Hosono, H. Enhanced critical-current in P-doped $BaFe_2As_2$ thin films on metal substrates arising from poorly aligned grain boundaries. *Sci. Rep.* **6,** 36828 (2016).

18. Norton, D. P. *et al.* Epitaxial $Yba_2Cu_3O_7$ on Biaxially Textured Nickel (001): An Approach to Superconducting Tapes with High Critical Current Density. *Science* **274,** 755–757 (1996).
19. Iijima, Y. Tanabe, N., Kohno, O. & Ikeno, Y. In-plane aligned $YBa_2Cu_3O_{7-x}$ thin films deposited on polycrystalline metallic substrates. *Appl. Phys. Lett.* **60,** 769–771 (1992).
20. Si, W. *et al.* Iron-chalcogenide $FeSe_{0.5}Te_{0.5}$ coated superconducting tapes for high field applications. *Appl. Phys. Lett.* **98,** 262509 (2011).
21. Si, W. *et al.* High current superconductivity in $FeSe_{0.5}Te_{0.5}$-coated conductors at 30 tesla. *Nat. Commun.* **4,** 1347 (2013).
22. Kasahara, S. *et al.* Evolution from non-Fermi- to Fermi-liquid transport via isovalent doping in $BaFe_2(As_{1-x}P_x)_2$. *Phys. Rev. B* **81,** 184519 (2010).
23. Shibauchi, T., Carrington, A. & Matsuda, Y. A Quantum Critical Point Lying Beneath the Superconducting Dome in Iron Pnictides. *Annu. Rev. Condens. Matter Phys.* **5,** 113–135 (2014).
24. Kawaguchi, T. *et al.* The strain effect on the superconducting properties of $BaFe_2(As,P)_2$ thin films grown by molecular beam epitaxy. *Supercond. Sci. Technol.* **27,** 065005 (2014).
25. Iida, K. *et al.* Hall-plot of the phase diagram for $Ba(Fe_{1-x}Co_x)_2As_2$. *Sci. Rep.* **6,** 28390 (2016).
26. Palstra, T. T. M., Batlogg, B., Schneemeyer, L. F. & Waszczak, J. V. Thermally Activated Dissipation in $Bi_{2.2}Sr_2Ca_{0.8}Cu_2O_{8+\delta}$. *Phys. Rev. Lett.* **61,** 1662–1665 (1988).
27. Thompson, J. R. *et al.* Vortex pinning and slow creep in high-J_c MgB_2 thin films: a magnetic and transport study. *Supercond. Sci. Technol.* **18,** 970–976 (2005).
28. Hänisch, J. *et al.* High field superconducting properties of $Ba(Fe_{1-x}Co_x)_2As_2$ thin films. *Sci. Rep.* **5,** 17363 (2015).
29. Uher, C., Cohn, J. L. & Schuller, I. K. Upper critical field in anisotropic superconductors. *Phys. Rev. B* **34,** 4906 (1986).
30. Klemm, R. A., Luther, A. & Beasley, M. R. Theory of the upper critical field in layered superconductors. *Phys. Rev. B* **12,** 877–891 (1975).
31. Tarantini, C. *et al.* Significant enhancement of upper critical fields by doping and strain in iron-based superconductors. *Phys. Rev. B* **84,** 184522 (2011).
32. Gurevich, A. Upper critical field and the Fulde-Ferrel-Larkin-Ovchinnikov transition in multiband superconductors. *Phys. Rev. B* **82,** 184504 (2010).
33. Gurevich, A. Iron-based superconductors at high magnetic fields. *Rep. Prog. Phys.* **74,** 124501 (2011).
34. Pan, A. V., Golovchanskiy, I. A. & Fedoseev, S. A. Critical current density: Measurements vs. reality. *EPL* **103,** 17006 (2013).
35. Tinkham, M. Introduction to Superconductivity. *Dover Publication, New York* 320 (2004).
36. Verebelyi, D. T. *et al.* Low angle grain boundary transport in $YBa_2Cu_3O_{7-\delta}$ coated conductors. *Appl. Phys. Lett.* **76,** 1755–1757 (2000).
37. Díaz, A., Mechin, L., Berghuis, P. & Evetts, J. E. Observation of viscous flux flow in $YBa_2Cu_3O_{7-\delta}$ low-angle grain boundaries. *Phys. Rev. B* **58,** R2960–R2963 (1998).
38. Daniels, G. A., Gurevich, A. & Larbalestier, D. C. Improved strong magnetic field performance of low angle grain boundaries of calcium and oxygen overdoped $YBa_2Cu_3O_x$. *Appl. Phys. Lett.* **77,** 3251–3253 (2000).
39. Fernández, L. *et al.* Influence of the grain boundary network on the critical current of $YBa_2Cu_3O_7$ films grown on biaxially textured metallic substrates. *Phys. Rev. B* **67,** 052503 (2003).
40. Xu, A. *et al.* Angular dependence of J_c for YBCO coated conductors at low temperature and very high magnetic fields. *Supercond. Sci. Technol.* **23,** 014003 (2010).
41. Li, G. Z. *et al.* Effects of carbon concentration and filament number on advanced internal Mg infiltration-processed MgB_2 strands. *Supercond. Sci. Technol.* **26,** 095007 (2013).
42. Boutboul, T. *et al.* Critical Current Density in Superconducting Nb-Ti Strands in the 100 mT to 11 T Applied Field Range. *IEEE Trans. Appl. Supercond.* **16,** 1184–1187 (2006).
43. Kanithi, H. *et al.* Production Results of 11.75 Tesla Iseult/INUMAC MRI Conductor at Luvata. *IEEE Trans. Appl. Supercond.* **24,** 6000504 (2014).
44. Parrell J. A. *et al.* High field Nb_3Sn conductor development at Oxford Superconducting Technology. *IEEE Trans. Appl. Supercond.* **13,** 3470–3473 (2003).
45. Parrell J. A., Field, M. B., Zhang, Y. & Hong, S. Nb_3Sn Conductor Development for Fusion and Particle Accelerator Applications. *AIP Conf. Proc.* **711,** 369 (2005).
46. Civale, L. *et al.* Scaling of the hysteretic magnetic behavior in $YBa_2Cu_3O_7$ single crystals. *Phys. Rev. B* **43,** 13732–13735 (1991).
47. Qin, M. J. *et al.* Paramagnetism and scaling behavior of flux pinning force density in a $GdBa_2Cu_3O_{6+x}$ thin film. *J. Appl. Phys.* **78,** 3287–3292 (1995).
48. Higuchi, T., Yoo, S. I. & Murakami, M. Comparative study of critical current densities and flux pinning among a flux-grown $NdBa_2Cu_3O_y$ single crystal, melt-textured Nd-Ba-Cu-O, and Y-Ba-Cu-O bulks. *Phys. Rev. B* **59,** 1514–1527 (1999).
49. Paturi, P., Malmivirta, M., Palonen, H. & Huhtinen, H. Dopant Diameter Dependence of $J_c(B)$ in Doped YBCO Films. *IEEE Trans. Appl. Supercond.* **26,** 8000705 (2016).
50. Dew-Hughes, D. Flux pinning mechanism in type II superconductors. *Philos. Mag.* **30,** 293–305 (1974).
51. Kramer, E. J. Scaling laws for flux pinning in hard superconductors. *J. Appl. Phys.* **44,** 1360–1370 (1973).
52. Díaz, A., Mechin, L., Berghuis, P. & Evetts, J. E. Evidence for Vortex Pinning by Dislocations in $YBa_2Cu_3O_{7-\delta}$ Low-Angle Grain Boundaries. *Phys. Rev. Lett.* **80,** 3855–3858 (1998).
53. Heinig, N. F., Redwing, R. D., Nordman, J. E. & Larbalestier, D. C. Strong to weak coupling transition in low misorientation angle thin film $YBa_2Cu_3O_{7-x}$ bicrystals. *Phys. Rev. B* **60,** 1409–1417 (1999).
54. Gurevich, A. *et al.* Flux Flow of Abrikosov-Josephson Vortices along Grain Boundaries in High-Temperature Superconductors. *Phys. Rev. Lett.* **88,** 097001 (2002).
55. Palau, A. *et al.* Correlation between grain and grain-boundary critical current densities in *ex situ* coated conductors with variable $YBa_2Cu_3O_{7-\delta}$ layer thickness. *Appl. Phys. Lett.* **88,** 122502 (2006).
56. Kończykowski, M. *et al.* Anisotropy of the coherence length from critical currents in the stoichiometric superconductor LiFeAs. *Phys. Rev. B* **84,** 180514 (2011).
57. van der Beek, C. J., Kończykowski, M. & Prozorov, R. Anisotropy of strong pinning in multi-band superconductors. *Supercond. Sci. Technol.* **25,** 084010 (2012).
58. Miura, M. *et al.* Strongly enhanced flux pinning in one-step deposition of $BaFe_2(As_{0.66}P_{0.33})_2$ superconductor films with uniformly dispersed $BaZrO_3$ nanoparticles. *Nat. Commun.* **4,** 2499 (2013).
59. Sheehan, C. *et al.* Solution deposition planarization of long-length flexible substrates. *Appl. Phys. Lett.* **98,** 071907 (2011).

Acknowledgements

A portion of this work was performed at the National High Magnetic Field Laboratory, which was supported by National Science Foundation Cooperative Agreement No. DMR-1157490, and the State of Florida. The work at Tokyo Institute of Technology was supported by the Ministry of Education, Culture, Sports, Science and Technology (MEXT) through Element Strategy Initiative to Form Core Research Center. K.I. acknowledges

support by the Japan Society for the Promotion of Science (JSPS) Grant-in-Aid for Scientific Research (B) Grant Number 16H04646. H.Hi was also supported by JSPS for Young Scientists (A) Grant Number 25709058, JSPS Grant-in-Aid for Scientific Research on Innovative Areas Nano Informatics (Grant Number 25106007), and Support for Tokyotech Advanced Research (STAR). We acknowledge support by Deutsche Forschungsgemeinschaft and Open Access Publishing Fund of Karlsruhe Institute of Technology.

Author Contributions

K.I., C.T., J.H., H.S. and H.Hi. designed the study and wrote the manuscript together with J.J. and H.Ho. Thin films preparation, structural characterisations and micro bridge fabrications were carried out by H.S. and H.Hi. K.I., C.T., J.H. and J.J. conducted high field transport measurements. C.T., H.S. and H.Hi. performed low field transport measurements. K.I., C.T., H.Hi. and H.Ho. supervised the projects. All authors discussed the results and implications and commented on the manuscript at all stages.

Additional Information

Supplementary information accompanies this paper at http://www.nature.com/srep

Competing financial interests: The authors declare no competing financial interests.

How to cite this article: Iida, K. *et al.* High-field transport properties of a P-doped $BaFe_2As_2$ film on technical substrate. *Sci. Rep.* **7**, 39951; doi: 10.1038/srep39951 (2017).

Publisher's note: Springer Nature remains neutral with regard to jurisdictional claims in published maps and institutional affiliations.